On the use of Contravariant Tensors to model Anisotropic Soft Tissues

Arthesh Basak[1], Amirtham Rajagopal[2], Umesh Basappa[3], and Mokarram Hossain[4]

[1]Department of Civil Engineering, GITAM Visakhapatnam, Andhra Pradesh, India.
[2]Department of Civil Engineering, IIT Hyderabad, Telangana, India.
[3]Department of Civil Engineering, NIT Warangal, Telangana, India.
[4]Zienkiewicz Centre for Computational Engineering (ZCCE), Swansea University, SA2 8EN, Swansea, United Kingdom.

1 Abstract

Biological tissues have been shown to behave isotropically at lower strain values, while at higher strains the fibres embedded in the tissue straighten and tend to take up the load. Thus, the anisotropy induced at higher loads can be mathematically modelled by incorporating the strains experienced by the fibres. Although existing works on modelling soft tissues using isotropic hyperelastic models have yielded satisfactory results, the behaviour of the tissue at higher loads can be more appropriately described by including anisotropic kinematic terms that account for the fibre strains at higher physiological loads. From histological studies on soft tissues it is evident that for a wide range of tissues the fibres have an oblique mean orientation about the physiological loading directions. Thus we require a mathematical framework of tensors defined in non-orthogonal basis to capture the direction-dependent response of fibres under high induced loads. In this work, we propose a novel approach to determine the fibre strains with the aid of the contravariant tensors defined in an oblique coordinate system. To determine the fibre strains, we introduce a fourth order contravariant *fibre orientation transformation tensor*.This helped us successfully determining the fibre strains, for a family of symmetrically and asymmetrically oriented fibres, with the aid of a single anisotropic invariant. Mathematical expressions for the Lagrangian and Eulerian stress definitions have been derived using continuum laws and the expression for the fourth order elasticity tensor has also been demonstrated. The proposed model was fitted with the experimental results from literature to determine the corresponding material parameters.

Keywords: Oblique coordinate system, Reciprocal basis, Anisotropic Hyperelasticity

2 Introduction

Mathematical models that give the relationships between physical quantities of a material are known as constitutive models. In solid mechanics, the constitutive laws concern relationships between various stresses and strains. A vast number of materials do not follow a linear relationship between the stresses and strains as is evident from the various experiments performed on the materials. Hyperelastic materials are examples of such kind which exhibit path-independent non linear behaviour. An example of such a material being rubber, see Treloar *et al.*[1]. Hyperelastic material models can primarily be grouped into two kinds as *Phenomological* models and *Micro-mechanical* models. Phenomenological models make use of complex forms of polynomial, exponential, logarithmic functions and so on to describe the material behaviour whereas micromechanical models use statistical mechanics of idealised chain molecules, see Steinmann *et al.* [2].

Hyperelastic materials can be modelled using direction independent *Isotropic* models or direction dependent *Anisotropic* approaches. Isotropic models generally are functions of the first three invariants of the right Cauchy-Green tensor. One of the simplest example of such is the neo-Hookean model [3] which uses a linear function of the first invariant of the right Cauchy-Green tensor. This invariant

based approach was used to extend a previously proposed model by Mooney [4], into a polynomial function of the first and the second invariants of the Cauchy-Green tensor and is commonly known as the Mooney-Rivlin model [3]. Yeoh [5] presented a n^{th} [n=1,2,3] order polynomial of the first invariant to model isotropic behaviour of incompressible materials. Another instance of the isotropic phenomenological model can be due to Ogden [6] which is a polynomial of the principal stretches. These isotropic models with polynomial forms have numerous applications in computational biomechanical studies like predicting the mechanical response of the brain during neurosurgery [7], identifying nodules in soft tissues to predict tumour [8], biomechanical behaviour of temporomandibular joints [9], wound rupture of skin etc [10]. Putra *et al.* [11] studied the performance of various hyperelastic material models for wearable biomedical devices and determined the suitability of the Yeoh model under biaxial extension tests.

Isotropic models with non polynomial functions are also present in the literature. Models of Delfino *et al.* [12] and Martins *et al.* [13] used a modified form of the Humphrey and Yin model [14] using exponential functions of the strain invariants. Mansouri and Darijani [15] also proposed an exponential function of the principal stretches and demonstrated its performance for rubber and biological tissues. Gsell *et al.* [16] applied exponential models to predict wall stresses and mechanical heart power in the left ventricle. Anisotropy in the material models can be induced using various forms of the functions of strains. Vaishnav *et al.*[17], Fung *et al.* [18],Takamizawa and Hayashi [19] have used polynomial, exponential, and logarithmic functions, respectively, of the Green-Lagrange strain tensor. For fibre reinforced hyperelastic materials, the constitutive model is expressed as a function of the fibre strains. A popular model of this type is the Holzapfel-Gasser-Ogden model *et al.* [20], commonly known as the HGO model which can be used effectively for the response of multilayered soft tissues. A modification to the HGO model was proposed by Nolan *et al.*[21] to correctly predict anisotropic compressible behaviour. Prediction of arterial behaviour with the inclusion of vascular smooth muscle was proposed by Zulliger *et al.* [22]. In the work by Cai *et al.* [23], a new strain energy function of the anisotropic invariants proposed by Ta *et al.* [24] was formulated and validated under various loading conditions. Holzapfel *et al.* [25] proposed two models based on the generalized structure tensor (GST) and angular integration(AI) and tested the performance of these models under uniaxial and biaxial extension of soft tissues. Recent works of Holzapfel and Ogden [26] proposed material models that include collagen content, cross linking of fibres and also proposed a model to capture damage for biological tissues [27]. Nakahara and Matsuda [28] proposed a new anisotropic hyperelastic model where the anisotropy is represented using modified Green-Lagrange strain like quantities. Limbert [29] reviewed various computational models for understanding the biophysics of the skin. Since micromechanical models are beyond the scope of the current work, the reader is advised to refer to the works of Chagnon *et al.* [30], Steinmann *et al.* [2], Hossain *et al.* [31, 32] for a comparative study of various popular micromechanical models.

From the aforementioned short review, we can conclude that the collagen fibres in soft tissues play a significant role in inducing direction dependent responses under mechanical loads. Therefore, the inclusion of the collagen fibre strains in the strain energy density function helps to model the realistic response of the soft tissues especially under high physiological loads. From histological studies [33] we can infer that the collagen fibres have an oblique mean orientation with respect to the main physiological loading directions. Therefore in order to determine the kinematic quantities in the fibre directions we would require a non-orthogonal oblique coordinate system aligned along the mean fibre directions.In this work we introduce a novel exponential model of the first invariant of anisotropic contravariant strain tensors that can capture the strains along the fibre directions oblique to the loading. For this purpose we propose the use of a fourth order *fibre orientation transformation tensor*.

This work is segmented with several sections 3 describing the motivation and mathematical framework leading to the formulation of the fourth order fibre orientation transformation tensor (section 3.4).This tensor leads to the proposal of a novel exponential model (section 5) from a continuum background described in section 4. Section 5 also demonstrates the expression for the stresses and derives the fourth order elasticity tensor which is implemented in section 6 to arrive at the discretized finite element formulation. These finite element equations are implemented using numerical examples in section 8 which have yielded good predictions when compared to the experimental results from literature.

3 Motivation for the current study

Mechanical strength of soft tissues are significantly governed by the presence and orientation of collagen fibres as they are the main load bearing components of soft tissues [20],[34].The distribution of the collagen fibres not only varies with the type of tissue but also varies along the depth of the tissue [35]. Collagen fibres have also been shown to have a significant role in the intralamellar bonding of tissues [36]. Histological studies have revealed that the seemingly disordered distribution of collagen fibres in a tissue, can actually be shown to have a mean orientation which are not aligned along the main loading directions of a tissue [37],[38],[33],[39]. These studies on the orientation of collagen fibres clearly reveal a general oblique alignment of the fibres with respect to the direction of loading. Thus to account for the strains in the direction of the fibres, which is the paramount for capturing the anisotropic behaviour, we propose a new model that expresses the continuum kinematic quantities in an oblique coordinate system with contravariant unit basis vectors parallel to the direction of the mean fibre orientation.

3.1 The necessity for a non-orthogonal basis

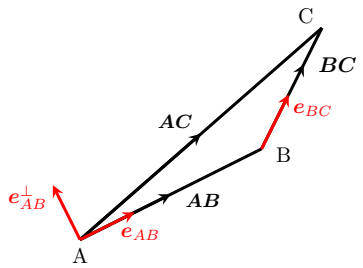

Figure 1: Vectors in equilibrium

Three vectors $\boldsymbol{AB}$, $\boldsymbol{BC}$ and $\boldsymbol{AC}$ as shown in Figure 1 form a closed triangle and thereby satisfying the parallelogram law of vector addition, i.e., $\boldsymbol{AC} = \boldsymbol{AB} + \boldsymbol{BC}$. Hence, it is evident that these vectors are in equilibrium. The objective is to determine the component of $\boldsymbol{AC}$ along the vectors $\boldsymbol{AB}$ and $\boldsymbol{BC}$. Using the trigonometry projection the components of $\boldsymbol{AC}$ along and across the $\boldsymbol{AB}$ are $|\boldsymbol{AC}|cos\theta$ and $|\boldsymbol{AC}|sin\theta$, respectively, that can mathematically be written as

$$\boldsymbol{AC} \;=\; |\boldsymbol{AC}\,|cos\theta\,\boldsymbol{e}_{AB} \;+\; |\boldsymbol{AC}|\,sin\theta\,\boldsymbol{e}^{\perp}_{AB} \tag{1}$$

wherein $\boldsymbol{e}_{AB}$ and $\boldsymbol{e}^{\perp}_{AB}$ are the unit vectors along and across the $\boldsymbol{AB}$. These components do not generate $\boldsymbol{AC}$ as the component $|\boldsymbol{AC}|sin\theta$ is not parallel to $\boldsymbol{BC}$, mathematically written as

$$\boldsymbol{AC} \;\neq\; |\boldsymbol{AC}\,|cos\theta\,\boldsymbol{e}_{AB} \;+\; |\boldsymbol{AC}|\,sin\theta\,\boldsymbol{e}_{BC} \tag{2}$$

wherein $\boldsymbol{e}_{BC}$ is the unit vector along $\boldsymbol{BC}$. The equality is achieved only when vectors are orthogonal, that is $\boldsymbol{AB}\cdot\boldsymbol{BC} = \boldsymbol{0}$. Therefore, the trigonometry projections of $\boldsymbol{AC}$ along non orthogonal vectors $\boldsymbol{AB}$ and $\boldsymbol{BC}$ shall not satisfy equilibrium equation. The subsequent sections will demonstrate the approach to determine these vectors using the contravariant oblique basis vectors.

3.2 Orthogonal coordinate system

A physical quantity can be described appropriately with the aid of rectangular coordinate system (RCS). The basis vectors most commonly used are the orthonormal basis. But not all quantities can be expressed easily with RCS as they might require non-orthogonal basis vectors. Such a coordinate system incorporating non-orthogonal basis is the oblique coordinate system (OCS). Referring to figure 2, let $\boldsymbol{X}_1$, $\boldsymbol{X}_2$ and $\boldsymbol{X}_3$ be the orthonormal basis in RCS. The unit oblique contravariant bases in the same space are $\boldsymbol{e}^1$, $\boldsymbol{e}^2$ and $\boldsymbol{e}^3$. The position vector $\boldsymbol{OA}$ can then be defined using both the coordinate systems as

$$\boldsymbol{OA} \;=\; \sum_{i=1}^{3} u_i \boldsymbol{X}_i \;=\; \sum_{j=1}^{3} v^j \boldsymbol{e}^j \tag{3}$$

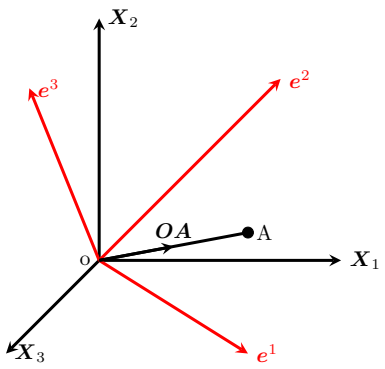

Figure 2: Rectangular and Oblique Coordinate Systems

where u_i are the components of $\boldsymbol{OA}$ along orthonormal basis $\boldsymbol{X}_i$ and v^j are the components along the oblique basis $\boldsymbol{e}^j$. It should be noted here that the orthonormal basis vectors will follow the general rule as $\boldsymbol{X}_i \cdot \boldsymbol{X}_j = \delta_{ij}$,where δ_{ij} is the *Kronecker Delta*, which will not be applicable for the oblique basis. So for working effectively using the oblique coordinate system, another set of basis known as the *Reciprocal Basis* is used. The scalar values v^j denote the magnitudes of the vector in the direction of e^j which together are in equilibrium with $\boldsymbol{OA}$. Now we will see how can we determine the components v^j.

3.3 Reciprocal basis

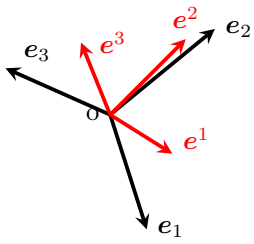

Figure 3: Oblique and Reciprocal Basis

Let us now define a set of right handed covariant basis vectors $\boldsymbol{e}_i$, which are related to the contravariant basis vectors $\boldsymbol{e}^j$ (refer figure 3) in such a manner that

$$\boldsymbol{e}_i \cdot \boldsymbol{e}^j = \delta_{ij} \tag{4}$$

where δ_{ij} represents the Kronecker Delta which essentially signifies that $\boldsymbol{e}_1$ is orthogonal to the plane containing $\boldsymbol{e}^2$ and $\boldsymbol{e}^3$ and is unity when dotted with $\boldsymbol{e}^1$. Such a set of basis vectors is called the *Reciprocal Basis* [40]. Hence the Reciprocal Basis written as

$$\boldsymbol{e}_k = \frac{\boldsymbol{e}^i \times \boldsymbol{e}^j}{\boldsymbol{e}^k \cdot [\boldsymbol{e}^i \times \boldsymbol{e}^j]} \tag{5}$$

3.4 Fibre Orientation Transformation Tensor

If we take the scalar product of equation 3 with the covariant basis $\boldsymbol{e}_k$ and use equation 4 we obtain

$$v^k = [\boldsymbol{e}_k \cdot \boldsymbol{X}_j]\, u_j. \tag{6}$$

Afterwards, the tensor $\boldsymbol{\alpha}$ from literature [40][41] with components α^i_j, is defined as

$$\boldsymbol{\alpha} = \alpha^i_j\, \boldsymbol{e}^i \otimes \boldsymbol{X}_j = [\boldsymbol{e}_i \cdot \boldsymbol{X}_j] \boldsymbol{e}^i \otimes \boldsymbol{X}_j \tag{7}$$

such that $\boldsymbol{\alpha}$ is the second order transformation tensor that converts the covariant components u_i of $\boldsymbol{OA}$ (figure 2) defined in RCS, to its contravariant components v^j defined in OCS. We now define a novel

fourth order transformation tensor $\boldsymbol{\beta}$ and name it *fibre orientation transformation tensor* which will transform a second order tensor A_{pq}, defined in RCS, to a transformed second order tensor B^{ij} defined in OCS such that

$$B^{ij}\,\boldsymbol{e}^i \otimes \boldsymbol{e}^j \;=\; \beta^{ij}_{kl}\,A_{kl}\,\boldsymbol{e}_k \otimes \boldsymbol{e}_l. \tag{8}$$

The components β^{ij}_{kl} can be determined as,

$$\beta^{ij}_{kl}\,\boldsymbol{e}^i \otimes \boldsymbol{e}^j \otimes \boldsymbol{X}_k \otimes X_l \;=\; \alpha^i_k\,\alpha^j_l\,\boldsymbol{e}^i \otimes \boldsymbol{e}^j \otimes \boldsymbol{X}_k \otimes \boldsymbol{X}_l. \tag{9}$$

The tensor β^{ij}_{pq} will be implemented later in section 5 to determine the strains in the directions of fibre orientations.

4 Continuum Mechanics Framework

Hyperelastic materials exhibit path independent behaviour as the deformation process can be solely described using the initial and the final state. As a result the material can be conceived with the use of a stored elastic potential Ψ which is a function of the deformation gradient $F_{iJ} = (\partial x_i/\partial \mathrm{X}_J)$, where x_i denotes the *Eulerian/Spatial* description of a *Lagrangian/Material* point X_J. Basically there are four different types of stresses that we encounter in continuum mechanics. These stresses provide significant information about the configuration or description in which they are defined. Hence there are two types of stresses for the Eulerian configuration namely the *Cauchy* stress tensor (σ_{ij}) and the *Kirchhoff* stress tensor (τ_{ij}). Similarly there exists two stress definitions in the Lagrangian configuration too, namely the *first Piola-Kirchhoff* stress tensor (P_{ij}) and the *second Piola-Kirchhoff* stress tensor (S_{ij}). An in-depth description of the various stress descriptions can be found in Lai *et al.*[42]. These stresses can be derived from the time derivative of Ψ as [43]

$$\dot{\Psi} \;=\; P_{ik}\dot{F_{ik}} \;=\; S_{ij}\dot{E_{ij}} \;=\; \frac{1}{2}\,S_{ij}\dot{C_{ij}} \tag{10}$$

where, $P_{ik} = \partial\Psi/\partial F_{ik}$ and $S_{ij} = \partial\Psi/\partial E_{ij}$ and the second order tensors C_{ij} and E_{ij} are the right *Cauchy-Green* tensor and *Lagrangian* or *Green* strain tensor, respectively, and are defined as

$$C_{ij} \;=\; F^T_{ik}\,F_{kj} \qquad E_{ij} \;=\; \frac{1}{2}\,[C_{ij} \,-\, \delta_{ij}] \tag{11}$$

The interrelationships between the various types of stresses are given below as

$$P_{ij} \;=\; J\sigma_{ik}F^{-T}_{kj} \qquad S_{ij} \;=\; F^{-1}_{ik}P_{kj} \qquad \tau_{ij} \;=\; J\sigma_{ij} \tag{12}$$

where $J = \det(F_{ij})$ is the Jacobian of the transformation tensor F_{ij}. In order to maintain objectivity of Ψ, a majority of times it is constructed as a function of C_{ij}. For modelling incompressible and nearly incompressible materials it is necessary to consider the volume preserving or isochoric component associated with right Cauchy-Green tensor. Thus C_{ij} can be made to undergo a multiplicative decomposition in which the isochoric part ($\bar{C}_{ij}$) is defined as

$$\bar{C}_{ij} \;=\; I_3^{-1/3}C_{ij} \tag{13}$$

and $I_3 = \det(C_{ij}) = J^2$ is the third invariant of the strain tensor C_{ij}. The strain energy density function Ψ too can be additively split as

$$\Psi \;=\; \Psi_{\mathrm{vol}} + \Psi_{\mathrm{isoch}} \tag{14}$$

Furthermore, for fibre reinforced composites, Ψ_{isoch} can be decomposed to consider the direction independent (isotropic) and direction independent (anisotropic) portions, respectively as

$$\Psi_{\mathrm{isoch}} \;=\; \Psi_{\mathrm{iso}} + \Psi_{\mathrm{aniso}}. \tag{15}$$

The isotropic component can be conceived to represent the strain energy density associated with the matrix of the composite. Hence Ψ_{iso} is generally written as a function of the frame independent invariants of $\bar{C}_{ij}$ so as to negate any directional preference. On the other hand, the anisotropic component Ψ_{aniso} is formulated in such a way so as to account for the straining of fibres.

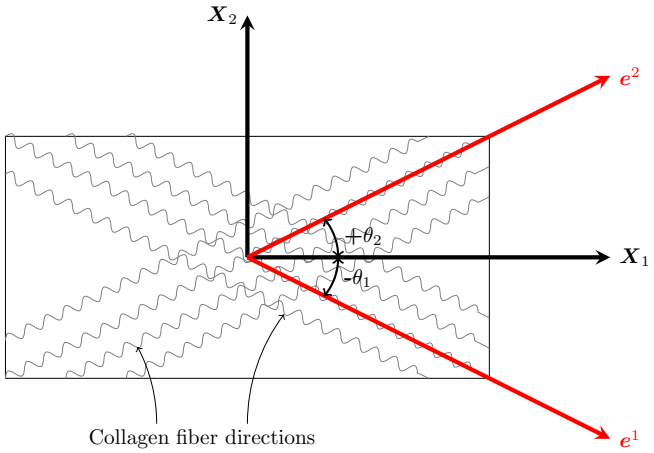

Figure 4: Family of obliquely aligned fibres w.r.t loading directions

5 Proposed Model

Fibre reinforced composites are generally an amalgamation of an isotropic matrix which is enhanced by the fibres. These fibres under strains give rise to directional responses. Generally composites, especially biological composites, are reinforced with two families of fibres placed symmetrically with respect to the an axis [33],[44]. Let us consider a fibre reinforced composite and let two orthogonal axes with orthonormal basis $\boldsymbol{X}_1$ and $\boldsymbol{X}_2$ be aligned along the major loading directions of the composite (figure 4). The orthonormal basis $\boldsymbol{X}_3$ is aligned orthogonal to the plane of the composite. Aligning unit contravariant oblique basis $\boldsymbol{e}^1$ and $\boldsymbol{e}^2$ along the two family of fibres and the third unit oblique basis $\boldsymbol{e}^3$ along $\boldsymbol{X}_3$ we can state that

$$\begin{bmatrix} \boldsymbol{e}^1 \\ \boldsymbol{e}^2 \\ \boldsymbol{e}^3 \end{bmatrix} = \begin{bmatrix} \cos\theta_1 & -\sin\theta_1 & 0 \\ \cos\theta_2 & \sin\theta_2 & 0 \\ 0 & 0 & 1 \end{bmatrix} \begin{bmatrix} \boldsymbol{X}_1 \\ \boldsymbol{X}_2 \\ \boldsymbol{X}_3 \end{bmatrix}$$

Using equations 5 and 7, we can derive the second order transformation tensor α^i_j and thereby formulate the fibre orientation transformation tensor defined in section 3.4 using equation 8 as

$$\beta^{ij}_{kl} = \alpha^i_k \, \alpha^j_l. \tag{16}$$

The fourth order tensor $\beta^{ij}_{kl}\,(\boldsymbol{e}^i \otimes \boldsymbol{e}^j \otimes \boldsymbol{X}_k \otimes \boldsymbol{X}_l)$ when applied to the second order isochoric tensor $\bar{C}_{ij}$ defined in equation 13 yields another second order tensor $\bar{C}^{*ij}$ such that

$$\bar{C}^{*ij}(\boldsymbol{e}^i \otimes \boldsymbol{e}^j) = \beta^{ij}_{kl}\,(\boldsymbol{e}^i \otimes \boldsymbol{e}^j \otimes \boldsymbol{X}_k \otimes \boldsymbol{X}_l)\,\bar{C}_{kl}(\boldsymbol{X}_k \otimes \boldsymbol{X}_l). \tag{17}$$

Hence the covariant modified right Cauchy-Green tensor $\bar{C}_{ij}$ that was defined using an orthogonal basis has been transformed, with the help of the fibre orientation transformation tensor β^{pq}_{ij}, to a contravariant tensor $\bar{C}^{*pq}$ with unit basis defined along the directions of fibre orientation. We can now determine the principal invariants of the tensor $\bar{C}^{*ij}$ as

$$\bar{I}^*_1 = \bar{C}^{*ij} I_{ij}, \qquad \bar{I}^*_2 = \bar{C}^{*ij}\bar{C}^{*ij}, \qquad \bar{I}^*_3 = \det(\bar{C}^{*ij}). \tag{18}$$

The first invariant $\bar{I}^*_1$ contains the sum of the square of the stretches along the fibre direction and hence can be used as an anisotropic strain measure. The derivative of $\bar{I}^*_1$ with respect to the isochoric $\bar{C}_{ij}$ can be computed as

$$\frac{\partial \bar{I}^*_1}{\partial \bar{C}_{ij}} = \alpha^i_k \alpha^j_k. \tag{19}$$

Now we use an exponential function as used by many previous literature [18],[12],[45] and define the anisotropic strain energy density function as

$$\Psi_{\text{aniso}} = \frac{\omega_1}{\omega_2}\left[e^{\omega_2[\bar{I}^*_1/\gamma - 1]^2} - 1\right] \tag{20}$$

where, $\gamma = \beta_{kl}^{ij}\delta_{kl}\delta_{ij}$ is the value $\bar{I}_1^*$ when no deformation occurs; $\omega_1 > 0$ is a parameter possessing the dimensions of stress and $\omega_2 > 0$ is a dimensionless parameter. The isotropic strain energy density function from various literature [45],[44] can be written as a neo-Hookean function as

$$\Psi_{\text{iso}} = \frac{\mu}{2}[\bar{I}_1 - 3] \tag{21}$$

where, the parameter $\mu > 0$ has the same dimensions as stress and $\bar{I}_1$ is the first invariant of $\bar{C}_{ij}$. Using the equations 20 and 21 in the expression 15 we can finally state

$$\Psi_{\text{isoch}} = \frac{\mu}{2}[\bar{I}_1 - 3] + \frac{\omega_1}{\omega_2}[e^{\omega_2[\bar{I}_1^*/\gamma - 1]^2} - 1]. \tag{22}$$

Hence Ψ_{isoch} becomes a function of the isotropic component $\bar{I}_1$ and the anisotropic component I_1^*.

$$\Psi_{\text{isoch}} = \Psi_{\text{iso}}(I_1) + \Psi_{\text{aniso}}(I_1^*). \tag{23}$$

5.1 Derivation of Stresses

From equation 10 we can determine the Lagrangian isochoric second Piola-Kirchhoff stress tensor as

$$S_{ij}^{\text{isoch}} = 2\frac{\partial \Psi_{\text{isoch}}}{\partial C_{ij}} \tag{24}$$

But Ψ_{isoch} is a function of $\bar{C}_{ij}$. Hence we can determine the isochoric second Piola-Kirchoff stress $\bar{S}_{ij}$ as

$$\bar{S}_{ij}^{\text{isoch}} = 2\frac{\partial \Psi_{\text{isoch}}}{\partial \bar{C}_{ij}}. \tag{25}$$

As discussed above in equation (15), $\bar{S}_{ij}^{\text{isoch}}$ can be further split as

$$\bar{S}_{ij}^{\text{isoch}} = \bar{S}_{ij}^{\text{iso}} + \bar{S}_{ij}^{\text{aniso}} \tag{26}$$

where,

$$\bar{S}_{ij}^{\text{iso}} = 2\frac{\partial \Psi_{\text{iso}}}{\partial \bar{C}_{ij}} \qquad \bar{S}_{ij}^{\text{aniso}} = 2\frac{\partial \Psi_{\text{aniso}}}{\partial \bar{C}_{ij}} \tag{27}$$

and S_{ij} can be derived from $\bar{S}_{ij}$ using the formula as given in Cheng and Zhang [46]:

$$S_{ij} = J^{-2/3}\mathbb{P}_{ijkl}\bar{S}_{kl} \tag{28}$$

where, $\mathbb{P}_{ijkl} = \mathbb{I}_{ijkl} - \frac{1}{3}C_{ij}^{-1} \otimes C_{kl} = \mathbb{I}_{ijkl} - \frac{1}{3}\bar{C}_{ij}^{-1} \otimes \bar{C}_{kl}$ and $\mathbb{I}_{ijkl}$ is the fourth order identity tensor. Furthermore, stress quantities can be written in the spatial configuration as

$$\sigma_{ij}^{\text{isoch}} = J^{-1}F_{ik}S_{kl}^{\text{isoch}}F_{jl}. \tag{29}$$

Hence the total Eulerian Cauchy stress tensor can be formulated as

$$\sigma_{ij} = -pI_{ij} + J^{-1}F_{ik}S_{kl}^{\text{isoch}}F_{jl} \tag{30}$$

where p is a Lagrange multiplier and $\boldsymbol{I}$ is the second order identity tensor.

5.2 Derivation of the Elasticity Tensor

The non-linear relationship between S_{ij} and C_{ij} needs to be linearized such that the Newton Raphson solution technique can be implemented. The linearization is carried using a fourth order Lagrangian or material elasticity tensor $\mathbb{C}_{ijkl}(\boldsymbol{X}_i \otimes \boldsymbol{X}_j \otimes \boldsymbol{X}_k \otimes \boldsymbol{X}_l)$ such that

$$DS_{ij}[u] = \mathbb{C}_{ijkl}DE_{kl}[u] \tag{31}$$

Where $DS_{ij}[u]$ and $DE_{kl}[u]$ are the directional derivatives of S_{ij} and E_{kl} in the direction $[u]$ [43]. The expression for $\mathbb{C}_{ijkl}$ can thus be derived as

$$\mathbb{C}_{ijkl} = \frac{\partial S_{ij}}{\partial E_{kl}} = 4\frac{\partial^2 \Psi}{\partial C_{ij}\partial C_{kl}} \tag{32}$$

The Eulerian or spatial elasticity tensor $\mathcal{C}_{ijkl}$ can be arrived from literature [43],[46] using the Piola push forward of $\mathbb{C}_{ijkl}$ as

$$\mathcal{C}_{ijkl} = J^{-1} F_{ip} F_{jq} F_{kr} F_{ls} \mathbb{C}_{pqrs} \tag{33}$$

6 Discretization of Equilibrium Equations

For arriving at the discretized equations of equilibrium we followed the method similar to the one derived in Rajagopal *et al.*[47]. Let $\mathfrak{N}_j(\boldsymbol{x})$ be the polynomial shape function at a node j with position $\boldsymbol{x}$. Thus for n number of total nodes in the discretized domain we can say:

$$x_i \;=\; \sum_{j=1}^{n} \mathfrak{N}_j(\boldsymbol{x}) x_{ji} \;=\; \mathfrak{N}_j \, x_{ji} \qquad\qquad \delta u_i \;=\; \sum_{j=1}^{n} \mathfrak{N}_j(\boldsymbol{x}) \, \delta u_{ji} \;=\; \mathfrak{N}_j \, \delta u_{ji} \tag{34}$$

In the above equation x_{ji} and δu_{ji} are the Eulerian position and displacement vector at the j^{th} node and for the i^{th} dimension. Thus we can describe the gradient of the displacement vector as

$$\frac{\partial \delta u_i}{\partial x_k} \;=\; \delta u_{k,i} \;=\; \sum_{j=1}^{n} \frac{\partial \mathfrak{N}_j(\boldsymbol{x})}{\partial x_k} \delta u_{ji} \;=\; D\mathfrak{N}_{k,j} \, \delta u_{ji} \tag{35}$$

We can write the weak statement of the equilibrium equation for a virtual displacement δu over the volume $\mathfrak{v}$ as

$$\delta W \;=\; \int_{\mathfrak{v}} \sigma_{ij,j} \, \delta u_i \, d\mathfrak{v}$$

Which when further simplified yields

$$\delta W \;=\; \int_{\mathfrak{v}} \sigma_{ij} \, \delta u_{i,j} \, d\mathfrak{v} \;-\; \int_{\mathfrak{a}} t_i \, \delta u_i d\mathfrak{a} \tag{36}$$

Using equations (34a & 34b) and (35) we can write the discretized form of δW as

$$\delta W \;=\; \int_{\mathfrak{v}} \delta u_{ik} \, D\mathfrak{N}_{k,j} \, \sigma_{ij} \, d\mathfrak{v} \;-\; \int_{\delta\mathfrak{a}} \delta u_{ij} \, \mathfrak{N}_j \, t_i \, d\mathfrak{a} \tag{37}$$

Considering the constitute relation derive in eq. 33, then above equation written as

$$\delta W \;=\; \int_{\mathfrak{v}} \delta u_{ik} \, D\mathfrak{N}_{k,j} \, \mathcal{C}_{ijlm} D\mathfrak{N}_{l,n} \, \delta u_{nm} \, d\mathfrak{v} \;-\; \int_{\delta\mathfrak{a}} \delta u_{ij} \, \mathfrak{N}_j \, t_i \, d\mathfrak{a} \tag{38}$$

Let $K_{iknm} \;=\; D\mathfrak{N}_{k,j} \, \mathcal{C}_{ijlm} D\mathfrak{N}_{l,n}$ be the element stiffness matrix, then the above equation written as

$$\delta W \;=\; \int_{\mathfrak{v}} \delta u_{ik} \, K_{iknm} \delta u_{nm} \, d\mathfrak{v} \;-\; \int_{\delta\mathfrak{z}} \delta u_{ij} \, \mathfrak{N}_j \, t_i \, d\mathfrak{a} \tag{39}$$

Expressing the above equation in matrix-vector form the equation is simplified to

$$\delta W \;=\; \boldsymbol{U}_i^T \, \boldsymbol{K}_{im} \, \boldsymbol{U}_m \;-\; \boldsymbol{U}_i^T \, \boldsymbol{T}_i \tag{40}$$

For equilibrium the $\delta W \;=\; 0$, which gives the relation

$$\boldsymbol{K}_{im} \, \boldsymbol{U}_m \;=\; \boldsymbol{T}_i \tag{41}$$

7 Proposed model in terms of principal stretches

The proposed strain energy density function, for an incompressible material, in terms of the principal stretches (λ_i) shall take the form

$$\Psi(\lambda_1, \lambda_2, \lambda_3) = 0.5\mu[\lambda_1^2 + \lambda_2^2 + \lambda_3^2 - 3] + \frac{\omega_1}{\omega_2} \left[e^{\omega_2 [I_1^*/\gamma - 1]^2} - 1\right] \tag{42}$$

Considering the mean fibre orientations $\theta_1 = \theta_2 = \theta$ then $I_1^* = \ell^2 \lambda_1^2 + m^2 \lambda_2^2$ is a function of in-plane stretches (λ_1,λ_2). The transformation parameters $\ell = sec\theta/\sqrt{2}$ and $m = cosec\theta/\sqrt{2}$ are obtained from

the fibre orientation transformation tensor $\boldsymbol{\beta}$. The scalar factor $\gamma = \ell^2 + m^2$ referring to the undeformed configuration.The components of the Cauchy stress can thus be obtained as

$$\sigma_i = \lambda_i \frac{\partial \Psi}{\partial \lambda_i}. \tag{43}$$

7.1 Uniaxial Extension

When a specimen is subjected to uniaxial extension, a unidirectional elongation ($\lambda_1 = \lambda$) is applied. The incompressibility condition ensures that $\lambda_1\lambda_2\lambda_3 = 1$ and hence the corresponding deformation gradient and the invariants take the form

$$\boldsymbol{F} = \begin{bmatrix} \lambda & 0 & 0 \\ 0 & \lambda^{-0.5} & 0 \\ 0 & 0 & \lambda^{-0.5} \end{bmatrix}, \quad I_1 = \lambda^2 + 2\lambda^{-1}, \quad I_1^* = \ell^2\lambda^2 + m^2\lambda^{-1}. \tag{44}$$

The Cauchy stress is determined as

$$\sigma_1 = 2\frac{\partial \Psi}{\partial I_1}[\lambda^2 - \lambda^{-1}] + \frac{\partial \Psi}{\partial I_1^*}[2\ell^2\lambda^2 - m^2\lambda^{-1}], \tag{45}$$

where

$$\frac{\partial \Psi}{\partial I_1} = \mu, \tag{46}$$

$$\frac{\partial \Psi}{\partial I_1^*} = \frac{2}{\gamma}\omega_1 e^{\omega_2[I_1^*/\gamma - 1]^2}[I_1^*/\gamma - 1]. \tag{47}$$

7.2 Equibiaxial Extension

In the case of a biaxial extension the specimen is stretched in two orthogonal directions. Applying the incompressibility condition we arrive at the deformation gradient and the corresponding invariants as

$$\boldsymbol{F} = \begin{bmatrix} \lambda_1 & 0 & 0 \\ 0 & \lambda_2 & 0 \\ 0 & 0 & (\lambda_1\lambda_2)^{-1} \end{bmatrix}, \quad I_1 = \lambda_1^2 + \lambda_2^2 + (\lambda_1\lambda_2)^{-2}, \quad I_1^* = \ell^2\lambda_1^2 + m^2\lambda_2^2. \tag{48}$$

In the case of an equibiaxial extension $\lambda_1 = \lambda_2 = \lambda$ and thus the corresponding components of the Cauchy stress can be determined as

$$\sigma_1 = 2\frac{\partial \Psi}{\partial I_1}[\lambda^2 - \lambda^{-4}] + 2\frac{\partial \Psi}{\partial I_1^*}[\ell^2\lambda^2], \tag{49}$$

$$\sigma_2 = 2\frac{\partial \Psi}{\partial I_1}[\lambda^2 - \lambda^{-4}] + 2\frac{\partial \Psi}{\partial I_1^*}[m^2\lambda^2]. \tag{50}$$

The derivatives of Ψ with respect to the invariants is determined using equations 46 and 47.The material constants μ, ω_1, ω_2 and θ are obtained after performing a curve fit with the experimental data. For the uniaxial loading condition, the model was fitted with the experimental data of extension of the arterial adventitia layer (specimen IX of Holzapfel *et al.*[44]) in the circumferential direction. The material constants for the equibiaxial condition were obtained by fitting the model to the experimental data from Niestrawska *et al.*[35] for abdominal aortic aneurysm in the circumferential and longitudinal directions. The circumferential stretch and longitudinal stretches were considered to be λ_1 and λ_2 respectively. Table 1 gives the values of the parameters obtained from curve fitting and the corresponding R^2 value illustrating the goodness of fit. The material constants thus obtained were used to plot the stress-stretch curve for both uniaxial and equibiaxial cases which showed good prediction with the experimental data as shown in figures 5 and 6.

7.3 The case of fibre asymmetry

The family of fibres can be asymmetrically aligned with respect to the loading directions (figure 4).Under such circumstances we can modify the strain energy function given in equation 42 in terms of principal invariants by taking $\ell^2 = (sin^2\theta_1 + sin^2\theta_2)/sin^2(\theta_1 + \theta_2)$ and $m^2 = (cos^2\theta_1 + cos^2\theta_2)/sin^2(\theta_1 + \theta_2)$ are obtained from the fibre orientation transformation tensor $\boldsymbol{\beta}$ after simplifications.The expression for Cauchy stress remains the same as given by equations 45,49 and 50.The expression of the derivative in equation 46 and 47 also remains unchanged.
It is interesting to note here that most popular anisotropic strain invariant models use two different invariants I_4 and I_6 to capture the fibre strains for asymmetrically aligned fibres. In case of the current proposed model we are able to integrate the fibre strains for asymmetric alignment of fibres ,with same material composition,with the help of the single parameter I_1^*/γ.
As there exists no experimental data ,to the best of our knowledge, for soft tissues embedded with asymmetrically oriented fibres, we used the numerical results of Holzapfel *et al.*[20] with material parameters $k_1 = k_3 = 4$ kPa and $k_2 = k_4 = 50$ for a qualitative comparison. The fibres were assumed to be oriented at $\theta_1 = 75^o$ and $\theta_2 = 30^o$. The equivalent material properties for the proposed model were determined as $\omega_1 = 6.3$ kPa and $\omega_2 = 97.9$. A neo-Hookean constant $\mu = 4$ kPa was used for both the models. Figure 7 shows the prediction from both the models under an uniaxial extension for the mentioned parameters. It is seen that the pseudo invariant I_1^*/γ gives an accurate prediction for the case of fibre asymmetry.

It is also interesting to note here that if the family of fibres is assumed to be aligned along the loading directions *viz* $\theta_1 = 0^o$ and $\theta_2 = 90^o$,then the second order transformation tensor $\boldsymbol{\alpha}$ becomes equal to $\boldsymbol{I}$, the second order identity tensor.Hence $\boldsymbol{\beta}$ does not transform the anisotropic invariant and therefore I_1^*/γ becomes equal to $I_1/2$,in two dimensional case,which induces direction independence in the material model.In figure 7 we can see that if $\boldsymbol{\beta}$ is inactivated by aligning the fibres along the principal loading directions, it is not possible to accurately predict the stresses for the same material parameters.Thus the inclusion of the anisotropic pseudo invariant I_1^*/γ ,arriving from the fibre orientation transformation tensor $\boldsymbol{\beta}$,is able to capture accurately the anisotropic response arising due to stretching of the fibres.Also for angles $\theta_1 = \theta_2 = 45^o$, it is worth observing that I_1^*/γ becomes equal to I_4.

Loading condition	Parameters	R^2
Uniaxial extension	$\mu = 3.05$ kPa	0.987
	$\omega_1 = 3.25$ kPa	
	$\omega_2 = 12.22$	
	$\theta = 75.30^o$	
Equibiaxial extension	$\mu = 2.5$ kPa	circumferential = 0.981 longitudinal = 0.958
	$\omega_1 = 2.85$ kPa	
	$\omega_2 = 37.5$	
	$\theta = 57.1^o$	

Table 1: Summary of material parameters and R^2 value for both loading conditions

8 Numerical examples

The proposed model was validated by implementing it in a finite element scheme.Two examples were considered (a) A square plate with a central hole under uniaxial extensions and (b) A homogeneous square plate under equibiaxial extension. From various literature [44],[25] it is evident that a combination of uniaxial and biaxial tests are necessary to accurately determine the material parameters of a constitutive relation thereby enhancing its predictive capability. A *Line Search* algorithm was implemented to arrive at the solution in finite number of incremental steps.

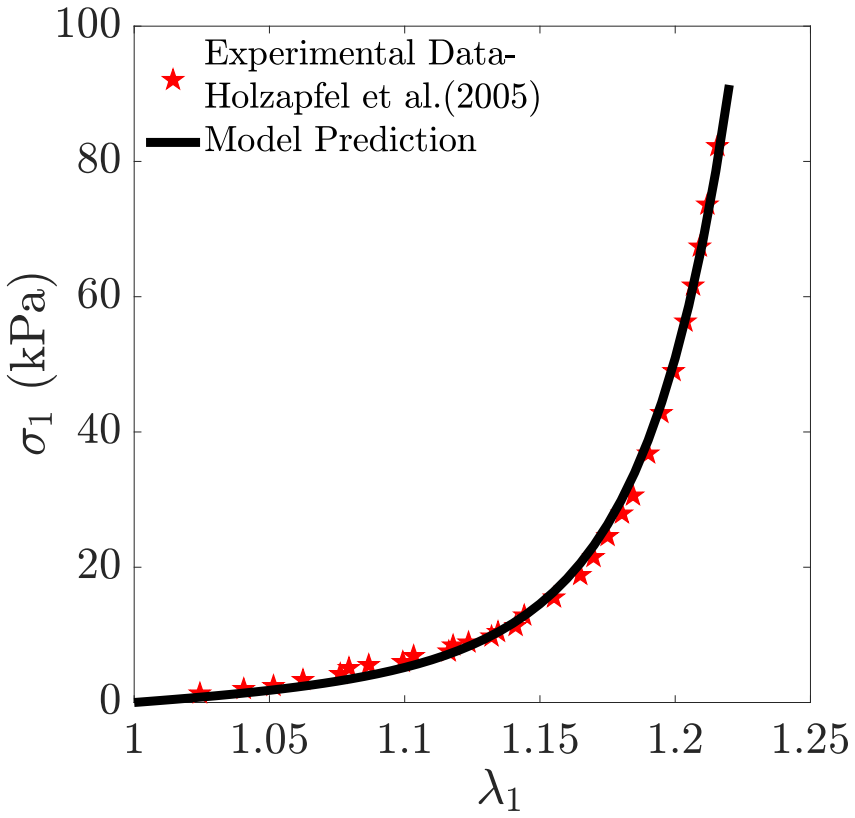

Figure 5: Horizontal stretch (λ_1) vs Horizontal Cauchy stress (σ_1)under uniaxial extension. The stars represent the circumferential experimental data from Holzapfel *et al.*[44].The smooth line represents the prediction of the proposed model

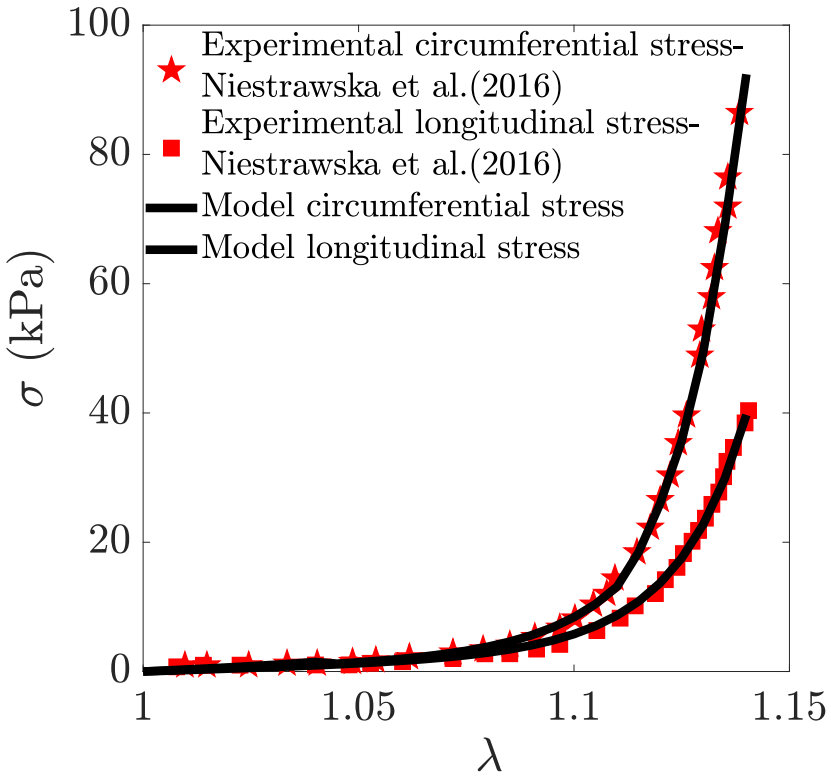

Figure 6: Stretch (λ) vs Cauchy stress (σ) under equibiaxial extension. The stars and squares represent the experimental data from Niestrawska *et al.*[35] for abdominal aortic aneurysm in the circumferential and longitudinal directions respectively. Smooth lines represent the prediction of the proposed model in the circumferential and longitudinal directions

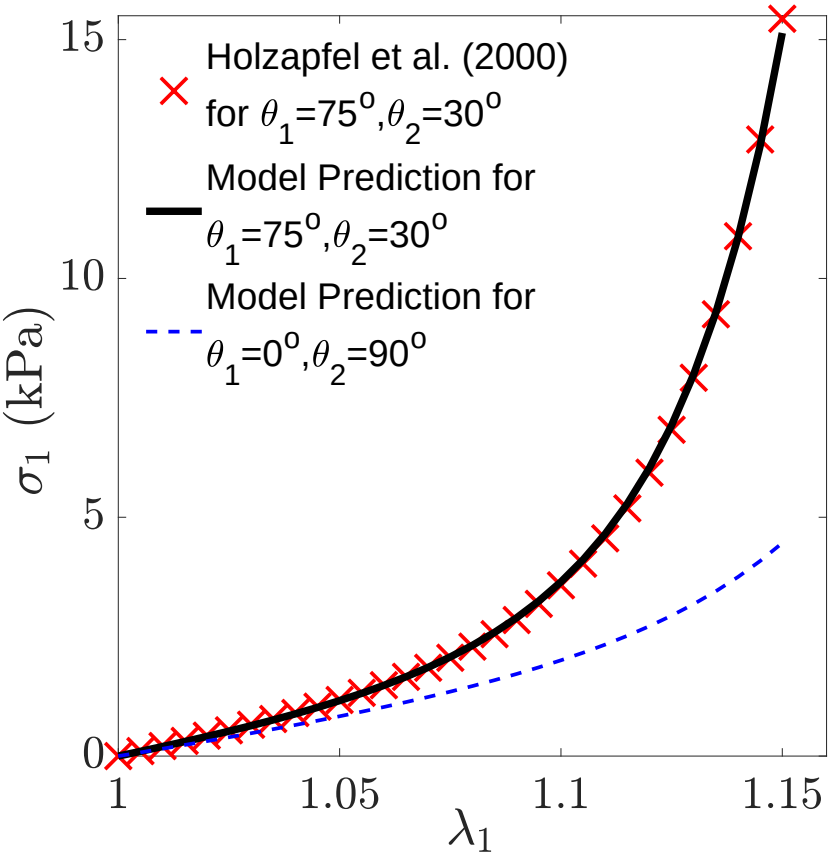

Figure 7: λ_1 vs σ_1 under uniaxial extension for a family of asymetrically oriented fibres. The 'X' represents the prediction of the model from Holzapfel *et al.*[20].The smooth line represents the prediction of the proposed model. The dashed line represents the prediction of the model for fibres oriented along the loading directions.

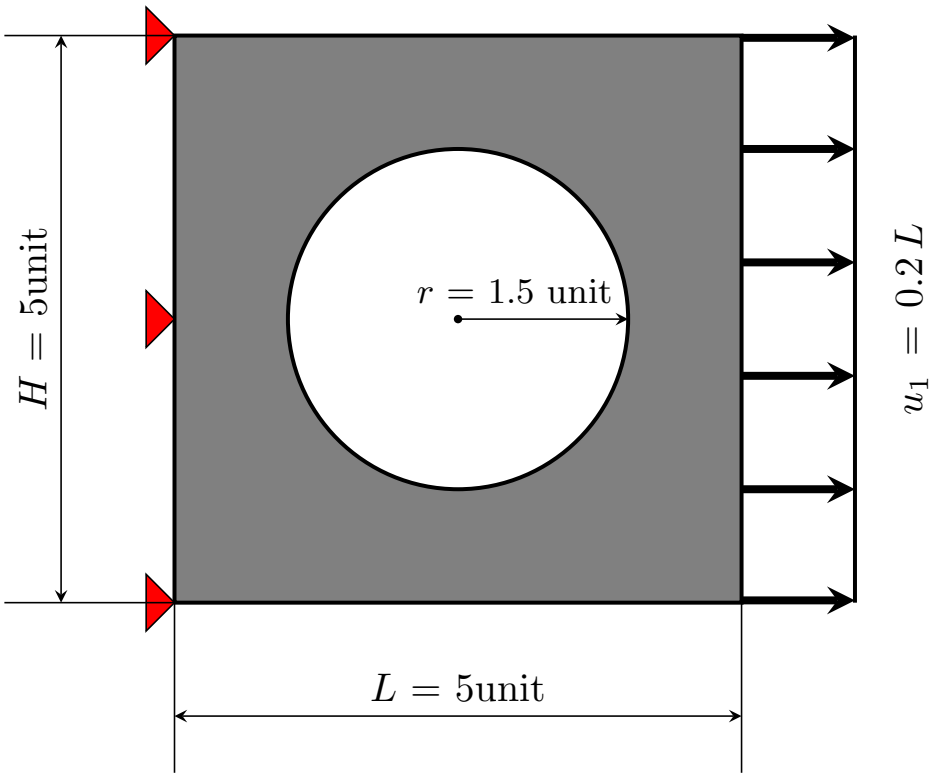

Figure 8: Square plate with a central hole under uniaxial extension in the horizontal direction

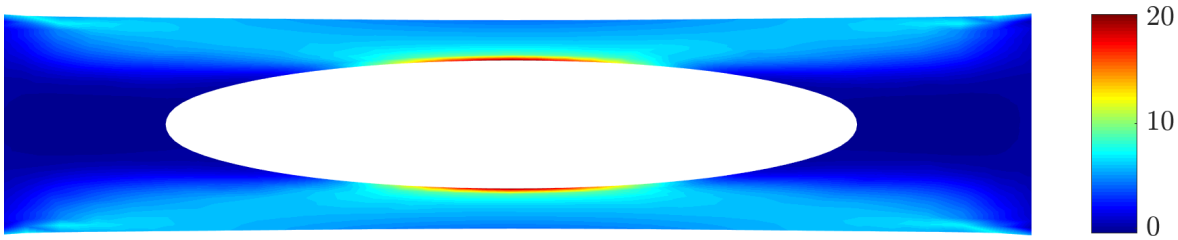

Figure 9: Horizontal Cauchy stress σ_1 (in kPa) contour under uniaxial extension

8.1 Uniaxial Extension

A square plate of dimensions $L = H = 5mm$ with a central hole of radius $r = 1.5mm$ was taken as shown in Figure 8.The plate was meshed using 4 noded quadrilateral elements. Quadratic mesh convergence was achieved at 765 elements. The material parameters were chosen from table 1. The material was considered to be nearly incompressible.The load was applied by fixing all nodes at one end of the plate and applying a stretch of 20 percent of the length in the horizontal direction to simulate the experimental boundary conditions [48].The contour of horizontal stress (σ_1) is shown in Figure 9

8.2 Equibiaxial Extension

Equibiaxial extension is a test that is commonly carried out to determine the bidirectional properties of a hyperelastic material.The test specimen is attached to clamps and pulled along the two axes of loading [49]as shown in Figure 10. A homogeneous square plate of dimensions $L = H = 5mm$ was meshed using 256, 4 noded, quadrilateral elements.The parameters for the proposed model were chosen from table 1. Seven nodes (symmetrically chosen) along each edge were stretched in the horizontal and vertical directions upto 12 percent.This was attempted to recreate the clamping procedure associated with equibiaxial tests [50]. Figure **??**(b) shows the deformed mesh after application of equibiaxial extension.

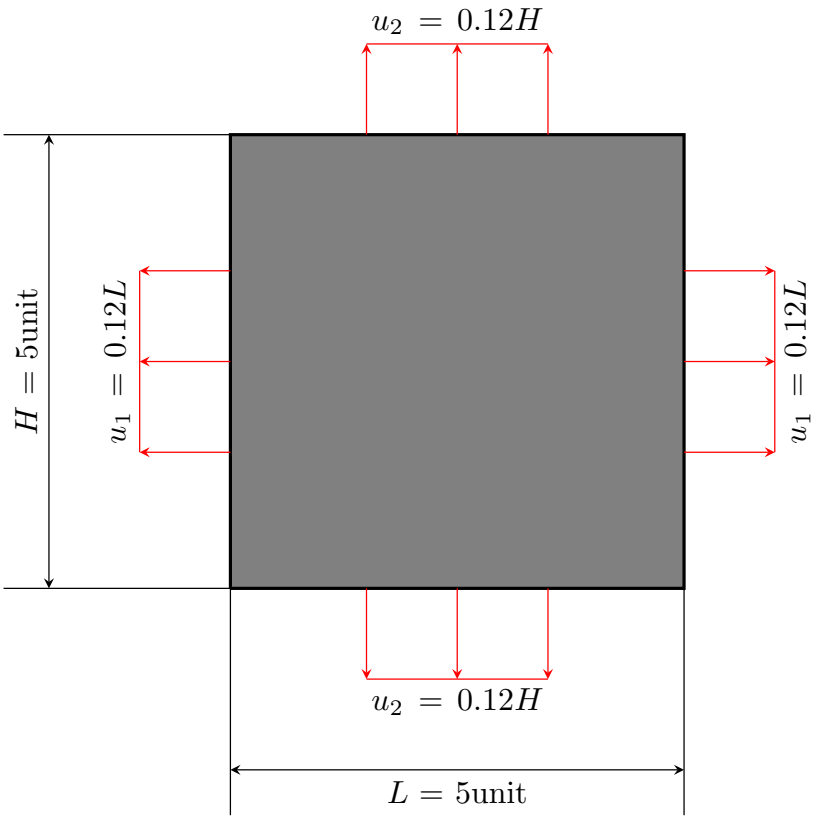

Figure 10: Square plate under equibiaxial extension

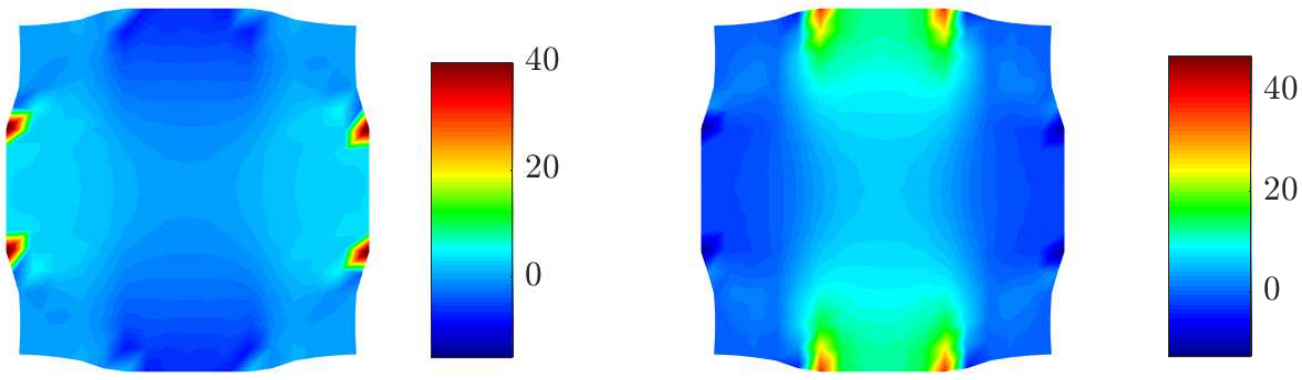

(a) (b)

Figure 11: (a) σ_1 (in kPa) and (b) σ_2 (in kPa) contour for a square plate under equibiaxial extension

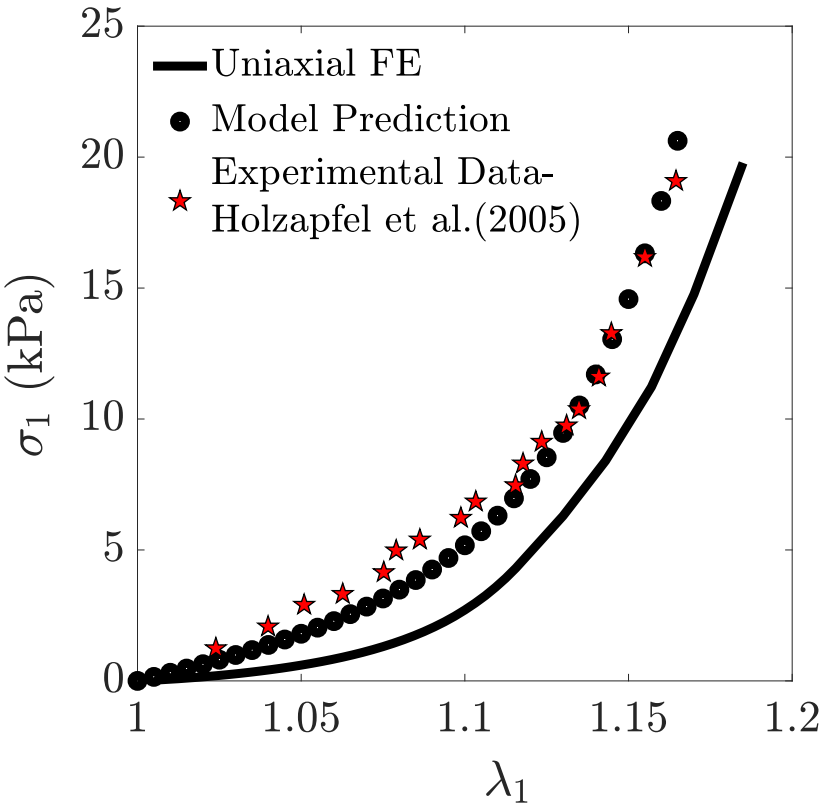

Figure 12: λ_1 vs σ_1 (in kPa) under uniaxial extension. The stars represent the experimental data from Holzapfel et al.[44]. The smooth line represents the prediction of the proposed model from FE analysis and the dots represent model prediction from equation 45

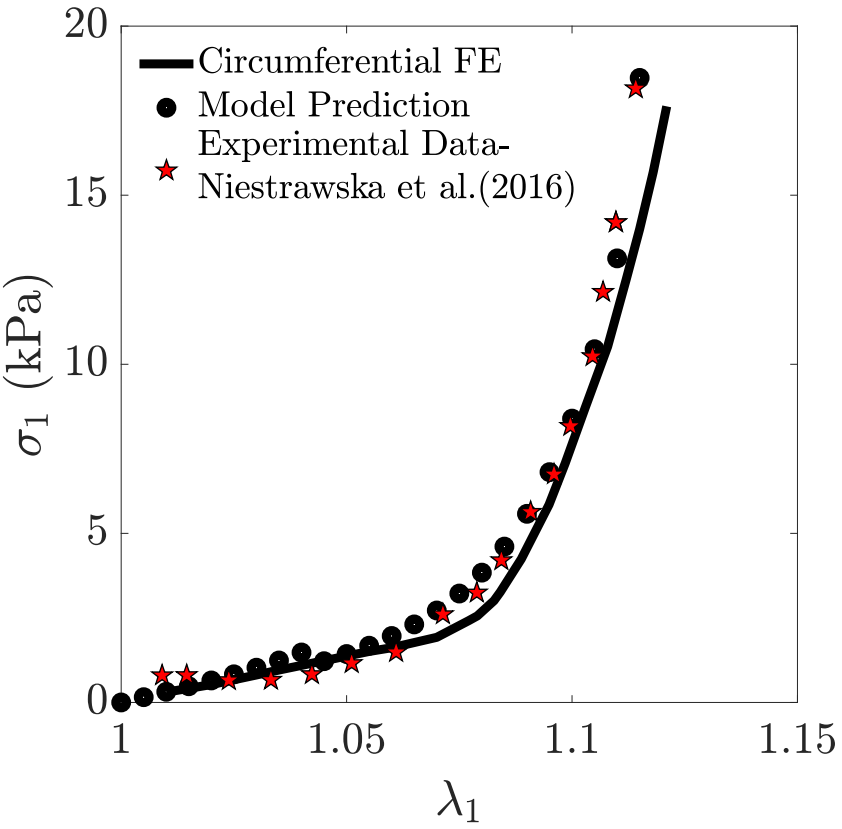

Figure 13: λ_1 vs σ_1 (in kPa)under equibaiaxial extension. The stars represent the circumferential experimental from Niestrawska *et al.*[35]. The smooth line represents the prediction of the proposed model from FE analysis and the dots represent model prediction from equation 49

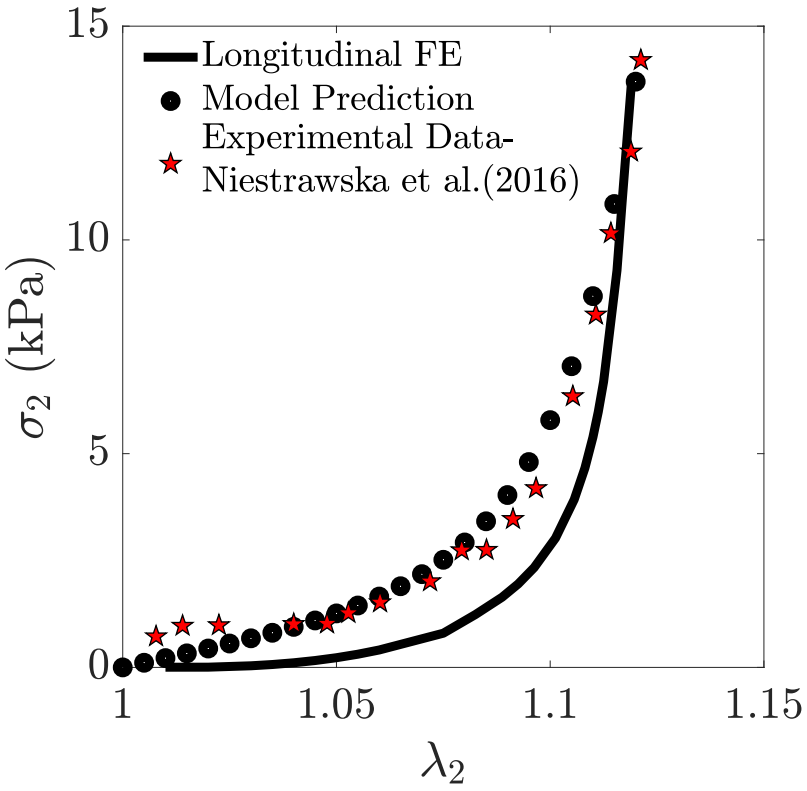

Figure 14: λ_2 vs σ_2 (in kPa) under equibaiaxial extension. The stars represent the longitudinal experimental data from Niestrawska *et al.*[35].The smooth line represents the prediction of the proposed model from FE analysis and the dots represent model prediction from equation 50

The contour for Cauchy stress in horizontal and vertical directions is shown in Figure 11.

9 Discussions and Conclusion

For the square plate with a hole under uniaxial extension a bulk modulus (κ) = 300kPa was used.This resulted in the material exhibiting a Poisson's Ratio (ν) $\approx$ 0.254. The stress concentration factor at the hole was observed to be $\approx$ 38 for a horizontal stretch of 1.20 (Figure 9) for the proposed model. Figure 12 depicts the response from the FE analysis of the proposed model with respect to the experimental results of Holzapfel *et al.*[44]. A bulk modulus (κ) = 50kPa was used for the FE analysis of the square plate under equibiaxial extension. Figures 13 and 14 show the prediction from the FE analysis in both the horizontal and vertical directions respectively as compared with the experimental data [35] .
The R^2 value from the FE prediction of the uniaxial extension of the square plate with a hole was determined as 0.987.For the square plate under equibiaxial extension the R^2 value was determined as 0.981 in the horizontal (circumferential) direction and 0.958 in the vertical (longitudinal) direction. Table 1 shows the summary of material parameters and the corresponding R^2 values.

Thus the current work presented an anisotropic hyperelastic material model with a novel approach for determining the fibre strains.This approach has been shown to be accurate in capturing the fibre strains for both symmetrically and asymmetrically placed two families of fibres as it reduces the computational time and model complexity by taking a single strain invariant I_1^* to determine the effect of fibre stretches in both directions. The proposed model was found to efficiently agree with the experimental data under uniaxial and biaxial loading conditions from literature, which are customary during the laboratory testing of hyperelastic materials. The response of the model under both uniaxial and biaxial extension displayed convexity of the function[30]. The elasticity tensor determined from equation 33 had a very robust performance when implemented in the Newton Raphson iterative scheme. Fitting the model to different kinds of experiments will generate better values of the coefficients. This will give rise to a better prediction and truncate the error further. Use of better fitting techniques may also result in more judicious predictions. Further investigations need to be carried out to determine the performance of the model in predicting the behaviour of other soft tissues.

References

[1] LRG Treloar. Stress-strain data for vulcanized rubber under various types of deformation. *Rubber Chemistry and Technology*, 17(4):813–825, 1944.

[2] Paul Steinmann, Mokarram Hossain, and Gunnar Possart. Hyperelastic models for rubber-like materials: consistent tangent operators and suitability for treloars data. *Archive of Applied Mechanics*, 82(9):1183–1217, 2012.

[3] RS Rivlin. Large elastic deformations of isotropic materials IV. Further developments of the general theory. *Philosophical Transactions of the Royal Society of London. Series A, Mathematical and Physical Sciences*, 241(835):379–397, 1948.

[4] Melvin Mooney. A theory of large elastic deformation. *Journal of Applied Physics*, 11(9):582–592, 1940.

[5] Oon H Yeoh. Characterization of elastic properties of carbon-black-filled rubber vulcanizates. *Rubber Chemistry and Technology*, 63(5):792–805, 1990.

[6] R. W Ogden. *Non-linear elastic deformations*. Dover Publications,INC. New York, 1997.

[7] Karol Miller, Grand R Joldes, George Bourantas, Simon K Warfield, Damon E Hyde, Ron Kikinis, and Adam Wittek. Biomechanical modeling and computer simulation of the brain during neurosurgery. *International Journal for Numerical Methods in Biomedical Engineering*, 35(10):e3250, 2019.

[8] Antonio Candito, Javier Palacio-Torralba, Elizabeth Jiménez-Aguilar, Daniel W Good, S Alan McNeill, Robert L Reuben, and Yuhang Chen. Identification of tumor nodule in soft tissue-an inverse finite-element framework based on mechanical characterization. *International Journal for Numerical Methods in Biomedical Engineering*, 36(8):e3369, 2020.

[9] Jingheng Shu, Hedi Ma, Lirong Jia, Hongyang Fang, Desmond YR Chong, Tinghui Zheng, Jie Yao, and Zhan Liu. Biomechanical behaviour of temporomandibular joints during opening and closing of the mouth: A 3d finite element analysis. *International Journal for Numerical Methods in Biomedical Engineering*, 36(8):e3373, 2020.

[10] Digendranath Swain and Anurag Gupta. Mechanics of cutaneous wound rupture. *Journal of Biomechanics*, 49(15):3722–3730, 2016.

[11] Ketut B Putra, Xiaoqing Tian, Jeffrey Plott, and Albert Shih. Biaxial test and hyperelastic material models of silicone elastomer fabricated by extrusion-based additive manufacturing for wearable biomedical devices. *Journal of the Mechanical Behavior of Biomedical Materials*, 107:103733, 2020.

[12] A Delfino, N Stergiopulos, JE Moore Jr, and J-J Meister. Residual strain effects on the stress field in a thick wall finite element model of the human carotid bifurcation. *Journal of Biomechanics*, 30(8):777–786, 1997.

[13] JAC Martins, EB Pires, R Salvado, and PB Dinis. A numerical model of passive and active behavior of skeletal muscles. *Computer Methods in Applied Mechanics and Engineering*, 151(3-4):419–433, 1998.

[14] JD Humphrey and FC Yin. On constitutive relations and finite deformations of passive cardiac tissue: I. a pseudostrain-energy function. *Journal of Biomechanical Engineering*, 109(4):298–304, 1987.

[15] MR Mansouri and H Darijani. Constitutive modeling of isotropic hyperelastic materials in an exponential framework using a self-contained approach. *International Journal of Solids and Structures*, 51(25-26):4316–4326, 2014.

[16] Matthias AF Gsell, Christoph M Augustin, Anton J Prassl, Elias Karabelas, Joao F Fernandes, Marcus Kelm, Leonid Goubergrits, Titus Kuehne, and Gernot Plank. Assessment of wall stresses and mechanical heart power in the left ventricle: Finite element modeling versus laplace analysis. *International Journal for Numerical Methods in Biomedical Engineering*, 34(12):e3147, 2018.

[17] Ramesh N Vaishnav, John T Young, and Dali J Patel. Distribution of stresses and of strain-energy density through the wall thickness in a canine aortic segment. *Circulation Research*, 32(5):577–583, 1973.

[18] YC Fung, K Fronek, and P Patitucci. Pseudoelasticity of arteries and the choice of its mathematical expression. *American Journal of Physiology-Heart and Circulatory Physiology*, 237(5):H620–H631, 1979.

[19] Keiichi Takamizawa and Kozaburo Hayashi. Strain energy density function and uniform strain hypothesis for arterial mechanics. *Journal of Biomechanics*, 20(1):7–17, 1987.

[20] Gerhard A Holzapfel, Thomas C Gasser, and Ray W Ogden. A new constitutive framework for arterial wall mechanics and a comparative study of material models. *Journal of Elasticity and the Physical Science of Solids*, 61(1):1–48, 2000.

[21] DR Nolan, AL Gower, M Destrade, RW Ogden, and JP McGarry. A robust anisotropic hyperelastic formulation for the modelling of soft tissue. *Journal of the Mechanical Behavior of Biomedical Materials*, 39:48–60, 2014.

[22] Martin A Zulliger, Alexander Rachev, and Nikos Stergiopulos. A constitutive formulation of arterial mechanics including vascular smooth muscle tone. *American Journal of Physiology-Heart and Circulatory Physiology*, 287(3):H1335–H1343, 2004.

[23] Renye Cai, Frédéric Holweck, Zhi-Qiang Feng, and François Peyraut. A new hyperelastic model for anisotropic hyperelastic materials with one fiber family. *International Journal of Solids and Structures*, 84:1–16, 2016.

[24] Anh-Tuan Ta, Frédéric Holweck, Nadia Labed, Alain Thionnet, and François Peyraut. A constructive approach of invariants of behavior laws with respect to an infinite symmetry group–application to a biological anisotropic hyperelastic material with one fiber family. *International Journal of Solids and Structures*, 51(21-22):3579–3588, 2014.

[25] Gerhard A Holzapfel, Ray W Ogden, and Selda Sherifova. On fibre dispersion modelling of soft biological tissues: a review. *Proceedings of the Royal Society of London Series A: Mathematical, Physical and Engineering Sciences*, 475(2224):20180736, 2019.

[26] Gerhard A Holzapfel and Ray W Ogden. An arterial constitutive model accounting for collagen content and cross-linking. *Journal of the Mechanics and Physics of Solids*, 136:103682, 2020.

[27] Gerhard A Holzapfel and Ray W Ogden. A damage model for collagen fibres with an application to collagenous soft tissues. *Proceedings of the Royal Society of London Series A: Mathematical, Physical and Engineering Sciences*, 476(2236):20190821, 2020.

[28] Hayato Nakahara and Akihiro Matsuda. Finite element computation with anisotropic hyperelastic model considering distributed fibers for artificial and natural leather used in sports. *Mechanical Engineering Journal*, 7(4):20–00072, 2020.

[29] Georges Limbert. Mathematical and computational modelling of skin biophysics: a review. *Proceedings of the Royal Society A: Mathematical, Physical and Engineering Sciences*, 473(2203):20170257, 2017.

[30] Grégory Chagnon, Marie Rebouah, and Denis Favier. Hyperelastic energy densities for soft biological tissues: a review. *Journal of Elasticity*, 120(2):129–160, 2015.

[31] Mokarram Hossain and Paul Steinmann. More hyperelastic models for rubber-like materials: consistent tangent operators and comparative study. *Journal of the Mechanical Behavior of Materials*, 22(1-2):27–50, 2013.

[32] Mokarram Hossain, AFMS Amin, and Muhammad Nomani Kabir. Eight-chain and full-network models and their modified versions for rubber hyperelasticity: a comparative study. *Journal of the Mechanical Behavior of Materials*, 24(1-2):11–24, 2015.

[33] Andreas J Schriefl, Georg Zeindlinger, David M Pierce, Peter Regitnig, and Gerhard A Holzapfel. Determination of the layer-specific distributed collagen fibre orientations in human thoracic and abdominal aortas and common iliac arteries. *Journal of the Royal Society Interface*, 9(71):1275–1286, 2012.

[34] A Whelan, J Duffy, RT Gaul, D OReilly, DR Nolan, P Gunning, C Lally, and BP Murphy. Collagen fibre orientation and dispersion govern ultimate tensile strength, stiffness and the fatigue performance of bovine pericardium. *Journal of the Mechanical Behavior of Biomedical Materials*, 90:54–60, 2019.

[35] Justyna A Niestrawska, Christian Viertler, Peter Regitnig, Tina U Cohnert, Gerhard Sommer, and Gerhard A Holzapfel. Microstructure and mechanics of healthy and aneurysmatic abdominal aortas: experimental analysis and modelling. *Journal of The Royal Society Interface*, 13(124):20160620, 2016.

[36] Ruizhi Wang, Xunjie Yu, and Yanhang Zhang. Mechanical and structural contributions of elastin and collagen fibers to interlamellar bonding in the arterial wall. *Biomechanics and Modeling in Mechanobiology*, pages 1–14, 2020.

[37] Nan Qi, Hao Gao, Raymond W Ogden, Nicholas A Hill, Gerhard A Holzapfel, Hai-Chao Han, and Xiaoyu Luo. Investigation of the optimal collagen fibre orientation in human iliac arteries. *Journal of the Mechanical Behavior of Biomedical Materials*, 52:108–119, 2015.

[38] RT Gaul, DR Nolan, and C Lally. Collagen fibre characterisation in arterial tissue under load using sals. *Journal of the Mechanical Behavior of Biomedical Materials*, 75:359–368, 2017.

[39] Markos Kapeliotis, Rebeca Alejandra Gavrila Laic, Alvaro Jorge Peñas, Jos Vander Sloten, Pieter Vanden Berghe, Nele Famaey, and Bart Depreitere. Collagen fibre orientation in human bridging veins. *Biomechanics and Modeling in Mechanobiology*, 19:2455–2489, 2020.

[40] Leonid P Lebedev, Michael J Cloud, and Victor A Eremeyev. *Tensor Analysis with Applications in Mechanics*. World Scientific, 2010.

[41] Eutiquio C Young. *Vector and Tensor Analysis*. CRC Press, 1992.

[42] W Michael Lai, David H Rubin, Erhard Krempl, and David Rubin. *Introduction to Continuum Mechanics*. Butterworth-Heinemann, 2009.

[43] Javier Bonet, Antonio J Gil, and Richard D Wood. *Nonlinear Solid Mechanics for Finite Element Analysis: Statics*. Cambridge University Press, 2016.

[44] Gerhard A Holzapfel, Gerhard Sommer, Christian T Gasser, and Peter Regitnig. Determination of layer-specific mechanical properties of human coronary arteries with nonatherosclerotic intimal thickening and related constitutive modeling. *American Journal of Physiology-Heart and Circulatory Physiology*, 289(5):H2048–H2058, 2005.

[45] Gerhard Holzapfel. *Biomechanics of Soft Tissue*. Academic Press, 2001.

[46] Jie Cheng and Lucy T Zhang. A general approach to derive stress and elasticity tensors for hyperelastic isotropic and anisotropic biomaterials. *International Journal of Computational Methods*, 15(04):1850028(1–33), 2018.

[47] Amirtham Rajagopal, Markus Kraus, and Paul Steinmann. Hyperelastic analysis based on a polygonal finite element method. *Mechanics of Advanced Materials and Structures*, 25(11):930–942, 2018.

[48] C Lally, AJ Reid, and Patrick J Prendergast. Elastic behavior of porcine coronary artery tissue under uniaxial and equibiaxial tension. *Annals of Biomedical Engineering*, 32(10):1355–1364, 2004.

[49] Amy A Claeson and Victor H Barocas. Planar biaxial extension of the lumbar facet capsular ligament reveals significant in-plane shear forces. *Journal of the Mechanical Behavior of Biomedical Materials*, 65:127–136, 2017.

[50] M Cilla, AV Corral, JA Peña, and E Peña. Analysis of the accuracy on computing nominal stress in a biaxial test for arteries. *Strain*, 56(1):e12331, 2020.